Photometric Lightcurves of Transneptunian Objects and Centaurs: Rotations, Shapes, and Densities

Scott S. Sheppard
Carnegie Institution of Washington

Pedro Lacerda
Grupo de Astrofisica da Universidade de Coimbra

Jose L. Ortiz
Instituto de Astrofisica de Andalucia

We discuss the transneptunian objects and Centaur rotations, shapes, and densities as determined through analyzing observations of their short-term photometric lightcurves. The lightcurves are found to be produced by various different mechanisms including rotational albedo variations, elongation from extremely high angular momentum, as well as possible eclipsing or contact binaries. The known rotations are from a few hours to several days with the vast majority having periods around 8.5 h, which appears to be significantly slower than the main-belt asteroids of similar size. The photometric ranges have been found to be near zero to over 1.1 mag. Assuming the elongated, high-angular-momentum objects are relatively strengthless, we find most Kuiper belt objects appear to have very low densities (<1000 kg m^{-3}) indicating high volatile content with significant porosity. The smaller objects appear to be more elongated, which is evidence of material strength becoming more important than self-compression. The large amount of angular momentum observed in the Kuiper belt suggests a much more numerous population of large objects in the distant past. In addition we review the various methods for determining periods from lightcurve datasets, including phase dispersion minimization (PDM), the Lomb periodogram, the Window CLEAN algorithm, the String method, and the Harris Fourier analysis method.

1. INTRODUCTION

The transneptunian objects (TNOs) are a remnant from the original protoplanetary disk. Even though TNOs may be relatively primitive, their spins, shapes, and sizes from the accretion epoch have been collisionally altered over the age of the solar system. The rotational distribution of the TNOs is likely a function of their size. In the current Kuiper belt the smallest TNOs (radii r < 50 km) are susceptible to erosion and are probably collisionally produced fragments (*Farinella and Davis,* 1996; *Davis and Farinella,* 1997; *Bernstein et al.,* 2004). These fragments may have been disrupted several times over the age of the solar system, which would have highly modified their rotational states (*Catullo et al.,* 1984). Intermediate-sized TNOs have probably been gravitationally stable to catastrophic breakup but are likely to have had their primordial rotations highly influenced through relatively recent collisions. The larger TNOs (r > 100 km) have disruption lifetimes longer than the age of the solar system and probably have angular momentum and thus spins that were imparted during the formation era of the Kuiper belt. Thus the largest TNOs may show the primordial distribution of angular momenta obtained through the accretion process while the smaller objects may allow us to understand collisional breakup of TNOs through their rotations and shapes.

Like the rotations, the shape distribution of TNOs is probably also a function of their size. The largest TNOs should be dominated by their gravity with shapes near their hydrostatic equilibrium point. The smaller TNOs are probably collisional fragments with self-gravity being less important, allowing elongation of the objects to dominate their lightcurves.

The main technique in determining the rotations and shapes of TNOs is through observing their photometric variability (*Sheppard and Jewitt,* 2002; *Ortiz et al.,* 2006; *Lacerda and Luu,* 2006). For the largest TNOs most photometric variations with rotation can be explained by slightly nonuniform surfaces. Two other distinct types of lightcurves stand out in rotation period and photometric range space for the largest TNOs (r > 100 km). The first type of lightcurve [examples are (20000) Varuna and (136108) 2003 EL_{61}] have large amplitudes and short periods that are indicative of rotationally elongated objects near hydrostatic

equilibrium (*Jewitt and Sheppard,* 2002; *Rabinowitz et al.,* 2006). The second type, of which only 2001 QG_{298} is a member to date, show extremely large amplitude and slow rotations and are best described as contact binaries with similar-sized components (*Sheppard and Jewitt,* 2004).

Two objects, (19308) 1996 TO_{66} and (24835) 1995 SM_{55}, may have variable amplitude lightcurves, which may result from complex rotation, a satellite, cometary effects, a recent collision, or most likely phase-angle effects (*Hainaut et al.,* 2000; *Sheppard and Jewitt,* 2003; *Belskaya et al.,* 2006; see also chapter by Belskaya et al.).

This chapter is organized as follows: In section 2 we discuss how rotation periods are determined from lightcurve observations and the possible biases involved. In section 3 the possible causes of the detected lightcurves are considered. In section 4 we mention what the measured lightcurves may tell us about the density and composition of the TNOs. In section 5 we look at what the shape distribution of the TNOs looks like when assuming that elongation is the reason for the larger lightcurve amplitudes and double-peaked rotation periods. In section 6 we discuss what the observed angular momentum of the ensemble of TNOs may tell us about the Kuiper belt's past environment. Finally, section 7 examines possible correlations between spin periods and amplitudes, and the dynamical and physical properties of the TNOs.

2. ANALYZING LIGHTCURVES

2.1. Period-Detection Techniques

There are currently several period-detection techniques such as phase dispersion minimization (PDM) (*Stellingwerf,* 1978), the Lomb periodogram (*Lomb,* 1976), the Window CLEAN algorithm (*Belton and Gandhi,* 1988), the String method (*Dworetsky,* 1983) and a Fourier analysis method (*Harris et al.,* 1989) that can be efficiently used to fit asteroid lightcurves. All these techniques are suitable to data that are irregularly spaced in time. Although the photometry data of TNOs are usually unevenly sampled, the sampling times are not random. This results in what is usually called "aliasing problems" (see section 2.3).

The PDM method (*Stellingwerf,* 1978) is especially suited to detect periodic signals regardless of the lightcurve shape. The PDM method searches for the best period that minimizes a specific parameter Θ. This parameter measures the dispersion (variance) of the data phased to a specific period divided by the variance of the unphased data. Therefore, the best period is the one that minimizes the dispersion of the phased lightcurve.

$$\Theta = s^2/\sigma^2 \tag{1}$$

where

$$\sigma^2 = \sum_{i=1}^{N} (x_i - \bar{x})^2/(N-1)$$

and

$$s^2 = \frac{\sum_{j=1}^{M} (n_j - 1)s_j^2}{\sum_{j=1}^{M} (n_j - M)}$$

N is the number of observations, x_i are the measurements, $\bar{x}$ is the mean of the measurements and s_j are the variances of M distinct samples. The samples are taken such that all the members have a similar ϕ_i, where ϕ_i is the phase corresponding to a trial period. Usually the phase interval (0,1) is divided into bins of fixed size, but the samples can be chosen in any other way that satisfies the criterion mentioned above.

The Lomb method (*Lomb,* 1976) is essentially a modified version of the well-known Fourier spectral analysis, but the Lomb technique takes into account the fact that the data are unevenly spaced and therefore the spectral power is "normalized" so that it weights the data in a "per point" basis instead of on a "per time" interval basis. The Lomb-normalized spectral power as a function of frequency $P_N(\omega)$ is

$$P_N(\omega) = \frac{1}{2\sigma^2}\frac{\left[\sum_j (h_j - \bar{h})\cos\omega(t_j - \tau)\right]^2}{\sum_j \cos^2\omega(t_j - \tau)} + \frac{\left[\sum_j (h_j - \bar{h})\sin\omega(t_j - \tau)\right]^2}{\sum_j \sin^2\omega(t_j - \tau)} \tag{2}$$

where ω is angular frequency ($2\pi f$), σ^2 is the variance of the data, $\bar{h}$ is the mean of the measurements, h_j and t_j are the measurements and their times, and τ is a kind of offset that makes $P_N(\omega)$ independent of shifting all the t_i by any constant. Quantitatively, τ is such that

$$\tan(2\omega\tau) = \sum_j \sin 2\omega t_j / \sum_j \cos 2\omega t_j$$

In this method, the best period is the one that maximizes the Lomb-normalized spectral power.

The String method (e.g., *Dworetsky,* 1983) finds the best period by searching for the period that minimizes a parameter that can be regarded as a length

$$L = \sum_{i=1}^{n} [(m_i - m_{i-1})^2 + (\Phi_i - \Phi_{i-1})^2]^{1/2} + [(m_i - m_n)^2 + (\Phi_i - \Phi_n + 1)^2]^{1/2} \tag{3}$$

where Φ_i are the phases from a trial period, m_i are the experimental values, and n is the number of observations.

The Window CLEAN algorithm (*Belton and Gandhi,* 1988) is a special application of the CLEAN algorithm (well known to radio astronomers, as it is widely used to synthesize images when dealing with synthetic aperture data). In the case of time series analysis, its application is made by computing a window function (which takes into account the observing times having zero value at the times when no data

were taken and 1 for the rest). This window function is used to deconvolve the true signal by means of the CLEAN algorithm. In other words, the window function is used to generate sort of a filter in the frequency domain to be applied to the regular Fourier spectrum in order to smooth out the spectral power of the signals that arise from the sampling pattern. Therefore the true periodic signal shows up more clearly in the corrected spectrum.

The Harris method (*Harris et al.,* 1989) was specifically developed for asteroid lightcurve studies and is basically a fit of the data to a Fourier series, which can be chosen to be of any degree

$$H(\alpha,t) = \bar{H}(\alpha) + \sum_{l=1}^{m} A_l \sin\frac{2\pi l}{P}(t - t_0) + B_l \cos\frac{2\pi l}{P}(t - t_0) \quad (4)$$

where $H(\alpha,t)$ is the computed magnitude at solar phase angle α and time t, $\bar{H}(\alpha)$ is the mean magnitude at phase angle α and A_1, B_1 are Fourier coefficients. For a given period P, the fit is carried out by finding the minimum of a bias-corrected variance

$$s^2 = \frac{1}{n-k}\sum_{i=1}^{n}\left(\frac{\delta_i}{\varepsilon_i}\right)^2$$

where $\delta_i = V_i(\alpha_j) - H(\alpha_j,t_i)$ is the deviation from the observations to the model (with α_j the phase angle of night j) and ε_i are *a priori* error estimates of the measurements. On the other hand, $k = 2m + p + 1$, where m is the degree of the Fourier series and p is the total number of days of data.

The minimum value of s^2 corresponds to the best solution. If increasing the degree of the solution by one fails to decrease s^2 by $s^2/(n - k)$, the new highest-order harmonic is taken as nonsignificant.

2.2. Computation of Significance Levels

After a period is identified by means of a suitable method one usually wants to know how confident that determination is. One of the nice features of the Lomb periodogram method is the fact that it readily gives a confidence level in the form $P(>z) = 1 - (1 - \exp - z)^M$ (*Scargle,* 1982) where z is the maximum spectral power and M is the number of independent frequencies, which can easily be estimated. In the case of the PDM method, the lower the value of Θ the higher the significance level. Although there is no formal expression for the significance in PDM a Θ value less than about 0.2 is desired in order for the found period to be considered highly significant. Other methods also give parameters that are associated to a significance level or give criteria to accept/reject periods, but in all cases it is assumed that the errors follow a Gaussian distribution.

The best approach to analyze the confidence levels may be by using Monte Carlo simulations. One can run Monte Carlo simulations in which one generates random photometry values within the range observed at exactly the same times as each data point was taken. The simulated datasets can be analyzed with the particular technique that the author has chosen and one can generate a distribution of values for, e.g., maximum Lomb-normalized spectral power or a distribution of values of minimum Θ or a distribution of the output of a given method. This distribution can be compared with the value from the analysis of the actual data and in that way one can assess a probability by comparing how many times a value larger/lower than a given threshold appeared in the simulation, divided by the number of simulations performed.

Unfortunately, the photometry errors are not completely random. Sometimes there are clear systematic errors that can be corrected for, but other times the systematic errors are not very evident. For instance, it is not unusual that photometry datasets from two different nights may have a small shift due to differential extinction (not adequately accounted for), or perhaps one night's data are noisier than another one because of larger seeing or extinction, or background source contamination may vary over a few hours. These systematic errors can also be simulated in Monte Carlo methods and therefore a more reliable confidence level can be computed.

When systematic errors are simulated, the confidence levels obtained always drop substantially compared to the case in which pure random errors were assumed. As an example, Fig. 1 depicts confidence levels for a real case using (1) Monte Carlo simulations in which only random Gaussian errors are assumed and (2) Monte Carlo simulations in which night-to-night random offsets of 0.03 variance are added to the otherwise random data.

Therefore, the inclusion of small 0.03-mag shifts in the data from different nights reveals that the spectral power can increase. In some cases these kind of systematic errors can give rise to periodicities that would be identified as signifi-

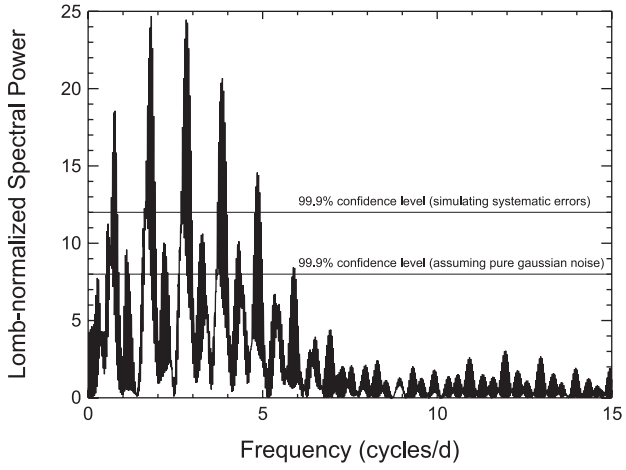

Fig. 1. Lomb Periodogram of Centaur (31824) Elatus (data from *Gutierrez et al.,* 2001). The main peak corresponds to the rotation period, whereas the other peaks are aliases at nearly 1 cycle/day spacing. Significance levels are indicated by the two horizontal lines (assuming two different error models).

cant by a regular Lomb periodogram in which the significance level was estimated by the equation $1 - (1 - \exp(-z))^M$.

2.3. Problems of Aliasing

As stated before, the data taken from a groundbased telescope are not randomly spaced in time, because there are more or less regular gaps in data acquisition sequences. For this reason there are inherent frequencies in the data that interfere with the true periodic variability of the object, giving rise to aliases. The main aliases are associated with the night-to-night observing gap and are such that

$$P_{alias}^{-1} = 1.0027\ d \pm P_{true}^{-1}$$

where 1.00027^{-1} is the length of the sidereal day.

Other minor aliases are seen at

$$P_{alias}^{-1} = k \times 1.0027\ d \pm P_{true}^{-1}$$

where k is an integer. See Fig. 1 as an example of a Lomb periodogram from a real case. The aliases are easy to identify when the plot is shown as a function of frequency instead of period, because of the ~1 spacing. These aliases usually have decreasing power as k increases. This is also illustrated in Fig. 1.

One can readily see that two waves $\exp(2\pi i f_1 t)$ and $\exp(2\pi i f_2 t)$ give the same samples at an interval Δ if and only if f_1 and f_2 differ by a multiple of $1/\Delta$.

When data are scarce, it is sometimes difficult to distinguish between the true period and an alias. Visual inspection of the lightcurve phased to one period or the other can sometimes help, but in some cases the ambiguity cannot be entirely resolved until more data are taken.

2.4. Selection Effects and Biases

Most of the TNO photometry reported is based on observations carried out in few-day observing runs, which implies that only short-term rotation variability can be detected. In addition, the photometry has some noise associated with it. Therefore, the current data sample may have some biases in the sense that short-term periods and large amplitudes are favored.

Unfortunately, long-term monitoring of TNOs (to try to debias the sample) is difficult to schedule in most telescopes as it requires many observing nights with medium-large telescopes. Besides, long-term monitoring requires careful absolute calibrations, which implies more observing time and photometric conditions that are not always met. Therefore, only a few cases have been studied. International collaboration to use different telescope resources would improve the situation and would also allow a better study of phase effects, which are important and sometimes might have caused misinterpretation of rotation periods due to opposition surges (see, e.g., *Belskaya et al.,* 2006). Also, the creation of a database where all TNO lightcurves could be accessible would allow to mitigate this problem. *Rousselot et al.* (2005a) have already created the infrastructure for that at the website *www.obs-besancon.fr/bdp/.*

3. CAUSES OF BRIGHTNESS VARIATIONS

Observed time-resolved photometric brightness variations of TNOs can be caused by several processes that may be periodic or variable (Fig. 2). A TNO's apparent magnitude is determined by its geometrical position relative to Earth and the Sun as well as its physical attributes and can be calculated from

$$m_R = m_\odot - 2.5\log[p_R r^2 \phi(\alpha)/2.25 \times 10^{16} R^2 \Delta^2)] \quad (5)$$

in which r [km] is the radius of the TNO, R [AU] is the heliocentric distance, Δ [AU] is the geocentric distance, $m_\odot$ is the apparent red magnitude of the Sun (–27.1), m_R is the apparent red magnitude of the TNO, p_R is the geometric albedo in the R band, and $\phi(\alpha)$ is the phase function, normalized in such a way that when $\alpha = 0°$ at opposition, $\phi(0) = 1$. The phase function depends on the surface properties of the object. For TNO lightcurve studies the rough approxi-

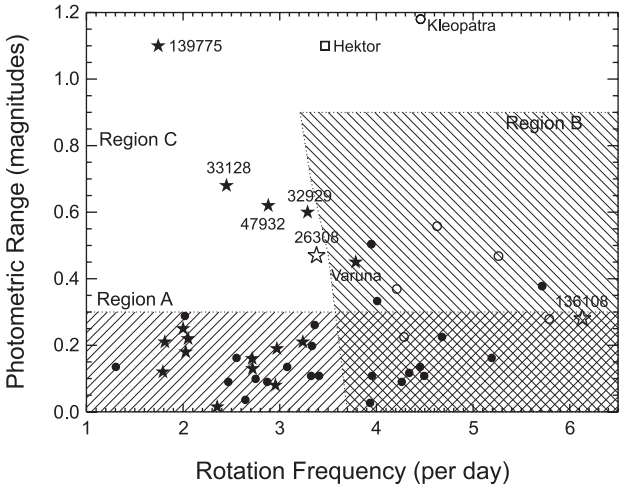

Fig. 2. Shown here are the rotation periods and photometric ranges of known TNO lightcurves and the main-belt asteroids with r > 100 km. Region A: The range of the lightcurve could be equally caused by albedo, elongation or binarity. Region B: The lightcurve range is most likely caused by rotational elongation. Region C: The lightcurve range is most likely caused by binarity of the object. Stars denote KBOs, circles denote main-belt asteroids (radii ≥ 100 km), and squares denote the Trojan 624 Hektor and the main-belt asteroid 216 Kleopatra, which are mentioned in the text. Open symbols signify known binary objects. Objects just to the left of Region B would have densities significantly less than 1000 kg m^{-3} in order to be elongated from rotational angular momentum. Binary objects are not expected to have photometric ranges above 1.2 mag. The TNOs that have photometric ranges below the photometric uncertainties (~0.1 mag) have not been plotted since their periods are unknown. These objects would all fall into Region A. The asteroids have been plotted at their expected mean projected viewing angle of 60° in order to more directly compare to the TNOs of unknown projection angle. Modified from *Sheppard and Jewitt* (2004).

mation $\phi(\alpha) = 10^{-0.4\beta\alpha}$ describes the linear phase dependence in magnitudes where β is the linear phase coefficient.

The brightness variations caused by the differing positional geometry of a TNO in equation (5) can usually be easily removed by simply using the absolute magnitude, defined as $m_R(1,1,\alpha) = m_R - 5\log(R\Delta) - \beta\alpha$, instead of the apparent magnitude. The absolute magnitude is the magnitude of the TNO if it were 1 AU from Earth and the Sun and at zero phase angle. The effects of differing heliocentric and geocentric distances are well understood, but the phase coefficient is not since it is dependent on the surface characteristics of the TNO (see chapter by Belskaya et al.).

3.1. Rotational Surface Variations

If a TNO has varying albedo or topography across its surface, the markings will cause a photometric lightcurve correlated with the object's rotation rate. For atmosphereless bodies, these surface variations usually do not create large-amplitude lightcurves and have been empirically found to be less than about 10–20% on most atmosphereless bodies (*Degewij et al.,* 1979; *Magnusson,* 1991). To date, no significant color variations with rotation have been observed from atmosphereless TNOs, which, if observed, may be an indication of compositional differences across the surface. The majority of low-amplitude lightcurves of large objects are believed to be caused by surface variations. Large objects able to substain atmospheres, such as Pluto, may obtain slightly higher albedo variations on their surfaces since dark areas will efficiently absorb light, creating warmth that may release volatiles into the atmosphere, which can then condense as bright spots on cooler surfaces (*Spencer et al.,* 1997).

3.2. Elongation from Material Strength

A TNO that is elongated will display photometric variations with rotation caused by changes in its projected cross-section. A rotationally elongated object will show a double-peaked lightcurve since each of two long and short axes will be observed during one full rotation. Assuming the lightcurve is produced from elongation of the object, we can use the maximum and minimum flux to determine the projection of the bodies' elongation into the plane of the sky through (*Binzel et al.,* 1989)

$$\Delta m = 2.5\log\left(\frac{a}{b}\right) - 1.25\log\left(\frac{a^2\cos^2\theta + c^2\sin^2\theta}{b^2\cos^2\theta + c^2\sin^2\theta}\right) \quad (6)$$

where $a \geq b \geq c$ are the semiaxes of a triaxial object with rotation about the c axis, Δm is the difference between the maximum and minimum flux expressed in magnitudes, and θ is the angle at which the rotation (c) axis is inclined to the line of sight (an object with $\theta = 90°$ is viewed equatorially).

Lightcurves of both asteroids and planetary satellites show that for the most part objects with radii ≥50 to 75 km have shapes mostly dominated by self-gravity and not by material strength (*Farinella,* 1987; *Farinella and Zappala,* 1997). This is attributed to the bodies having weak structures from fragmentation accrued in past harsh collisional environments (e.g., *Davis and Farinella,* 1997). Unlike the largest TNOs, the smaller TNOs are expected to not be dominated by self-gravity and thus may be structurally elongated. To date few small TNOs have been observed for rotational data, but they appear to have larger-amplitude lightcurves (*Trilling and Bernstein,* 2006).

It is assumed that the smaller TNOs have random pole orientations due to collisions, yet it remains to be seen if this is true for the largest TNOs. For a random distribution, the probability of viewing an object within the angle range θ to $\theta + d\theta$ is proportional to $\sin(\theta)d\theta$. Since the average viewing angle is one radian ($\theta \approx 60°$) the average sky-plane ratio of the axes of an elongated body is smaller than the actual ratio by a factor $\sin(60) \approx 0.87$. Collisionally produced fragments on average have axis ratios $2:2^{1/2}:1$ (*Fujiwara et al.,* 1978; *Capaccioni et al.,* 1984). When viewed equatorially, such fragments will have $\Delta m = 0.38$ mag. At the mean viewing angle $\theta = 60°$ we obtain $\Delta m = 0.20$ mag.

3.3. Rotational Elongation from High Angular Momentum

An object will fly apart if it reaches the critical rotational period, P_{crit}, when the centrifugal acceleration of a rotating body equals the gravitational acceleration. This occurs at

$$P_{crit} = \left(\frac{3\pi}{G\rho}\right)^{1/2} \quad (7)$$

where G is the gravitational constant and ρ is the density of the object. Even with longer rotation periods an object will be rotationally deformed. In the main-belt asteroids, only the smallest (~0.1 km-sized) asteroids have the tensile strength to resist rotational deformation (*Pravec et al.,* 2003). The amount of deformation depends on the structure and strength of the body. Strengthless rubble-pile-type structures become triaxial "Jacobi" ellipsoids at rotations just above the critical rotation point (*Chandrasekhar,* 1969; *Weidenschilling,* 1981). Since we can estimate the shape and specific angular momentum from the amplitude and rotation period of an object we can estimate their bulk densities (see section 4.1). Both lightcurves of the TNOs (20000) Varuna (*Jewitt and Sheppard,* 2002) and (136108) 2003 EL_{61} (*Rabinowitz et al.,* 2006) have been explained through rotational deformation, while several large main-belt asteroids have similar characteristics (*Farinella et al.,* 1981).

3.4. Eclipsing or Contact Binaries

Transneptunian object lightcurves could be generated from eclipsing or contact binaries. The wider the separation, the more distinctive or "notched" the expected lightcurve, unlike the more sinusoidal lightcurves caused by most other rotational effects. The axis ratio of 2:1, which is a contact

binary consisting of two equally sized spheres, corresponds to a peak-to-peak lightcurve range $\Delta m = 0.75$ mag, as seen from the rotational equator. Viewed at the average viewing angle of $\theta = 60°$ would give a lightcurve range of $\Delta m = 0.45$ mag. Very close binary components should be elongated by mutual tidal forces, giving a larger lightcurve range (*Leone et al.,* 1984). Leone et al. find that the maximum range for a tidally distorted nearly contact binary is about 1.2 mag. The contact binary hypothesis is the likely explanation of TNO 2001 QG_{298}'s lightcurve (*Sheppard and Jewitt,* 2004) as well as Jupiter Trojan (624) Hektor's lightcurve (*Hartmann and Cruikshank,* 1978; *Weidenschilling,* 1980; *Leone et al.,* 1984), and could also explain the lightcurve of main-belt asteroid (216) Kleopatra (*Leone et al.,* 1984; *Ostro et al.,* 2000; *Hestroffer et al.,* 2002).

3.5. Variable

Nonperiodic time-resolved photometric variations could be caused by a recent impact on the TNO's surface, a complex rotational state, a binary object that has different rotation rates for each component, or even cometary activity (*Hainaut et al.,* 2000). Impacts are thought to be exceedingly rare in the outer solar system and the probability that we would witness such an event is very small.

The timescale for a complex rotation state to damp to principal axis rotation (*Burns and Safronov,* 1973; *Harris,* 1994) is $T_{damp} \sim \mu Q/(\rho K_3^2 r^2 \omega^3)$ where μ is the rigidity of the material composing the asteroid, Q is the ratio of the energy contained in the oscillation to the energy lost per cycle, ρ is the bulk density of the object, ω is the angular frequency of the rotation, r is the mean radius of the object, and K_3^2 is the irregularity of the object in which a spherical object has $K_3^2 \sim 0.01$ while a highly elongated object has $K_3^2 \sim 0.1$. All TNOs and Centaurs observed to date are relatively large, and with reasonable assumptions about the other parameters, one finds all are expected to be in principal-axis rotation because the damping time from a complex rotational state is much less than the age of the solar system.

Because of the very long orbital periods for the TNOs (>200 yr) we don't expect the pole orientation to our line of sight to change significantly over the course of several years and thus we should not expect any significant lightcurve changes from differing pole orientations from year to year for TNOs. Centaurs may have shorter orbital periods and thus their pole orientation to our line of sight may significantly change over just a few years. A few attempts have been made at determining possible pole orientations for Centaurs from their varying lightcurve amplitudes (*Farnham,* 2001; *Tegler et al.,* 2005).

Cometary activity is not expected at such extreme distances from the Sun, although several attempts have been made to observe such processes with no obvious activity reported to date for objects beyond Neptune's orbit. Two TNOs have been reported to have possible variability, (19308) 1996 TO_{66} (*Hainaut et al.,* 2000) and (24835) 1995 SM_{55} (*Sheppard and Jewitt,* 2003). The reported variability of 1996 TO_{66} seems to have been caused by several observations obtained at very different phase angles (*Belskaya et al.,* 2006). The variability of 1995 SM_{55} has been suggested but not confirmed.

4. SPIN STATISTICS

4.1. Densities

It is widely believed that mutual collisions have significantly affected the inner structure of TNOs. Objects with radii r > 200 km have presumably never been disrupted by impacts, but have probably been increasingly fractured and gradually converted into gravitationally bound aggregates of smaller pieces (*Davis and Farinella,* 1997; Lacerda et al., in preparation). Whenever shaken by subsequent collisions, such pieces will progressively rearrange themselves into energetically more stable configurations, and the overall shape of the objects will relax to an equilibrium between gravitational and inertial accelerations (due to rotation). In contrast, smaller TNOs (r < 100 km) have probably been produced in catastrophic collisions between intermediate-sized (r ~ 100–200 km) bodies, and may be coherent fragments whose shapes depend mostly on material strength, or reaccumulations of impact ejecta (see, e.g., *Leinhardt et al.,* 2000). Indirect evidence for the latter comes from, e.g., the tidal disruption of Comet Shoemaker-Levy 9 (*Asphaug and Benz,* 1996, and references therein), which is believed to have originated in the transneptunian region (*Fernandez,* 1980; *Duncan et al.,* 1988). The very largest TNOs, which constitute a large fraction of the sample considered here, have also probably relaxed to equilibrium shapes as a consequence of high internal pressures (*Rabinowitz et al.,* 2006, and references therein).

If we assume that TNOs have relaxed to equilibrium shapes then their rotation states can be used to set limits on their densities: The centripetal acceleration due to self-gravity (bulk density) must be sufficient to hold the material together against the inertial acceleration due to rotation (spin period). In the extreme case of fluids, the balance of the two accelerations restricts the shapes of the rotating objects to certain well-studied figures of equilibrium (*Chandrasekhar,* 1969). Although TNOs are composed of solid material, their presumed fragmentary structure (or sheer size and internal pressure in the case of the largest bodies) validates the fluid approximation as a limiting case, which we will assume as valid in the remainder of this section [i.e., we ignore any friction that may change their shapes slightly (*Holsapple,* 2001, 2004)].

The figures of equilibrium that produce lightcurves are the Jacobi ellipsoids since they are triaxial. Assuming an equator-on geometry, we can use equation (6) with the measured peak-to-peak amplitude of a lightcurve to calculate a lower limit for the a/b axis ratio of the Jacobi ellipsoid that best approximates the shape of the TNO. Chandrasekhar's

formalism relates the shape and spin period of the TNO to its density [see *Chandrasekhar* (1969) for an in-depth analysis of the simple density relation shown in equation (7)]. Since the estimated a/b is a lower limit, due to the unknown geometry, the derived density will also be a lower limit. An upper limit can also be obtained from the fact that ellipsoids with a/b > 2.31 are unstable to rotational fission (*Jeans,* 1919).

In Fig. 3 we plot density ranges, calculated as described above, vs. $m_R(1,1,0)$ for TNOs brighter than absolute magnitude 6 (r > 100 km assuming moderate albedos), more likely to be figures of equilibrium (safely in the gravity dominated regime, with clear double-peaked lightcurves, and spin period P < 10 h). Also shown are TNOs Pluto, Charon, and 1999 TC_{36}, which belong to multiple systems and are thus suitable for density measurement (see chapter by Noll et al.). A trend of larger (brighter) objects being denser is apparent. This trend can be attributed to porosity (volume fraction of void space), to rock/ice mass fraction, or to a combination of both. Indeed, bodies with density lower than water must have some internal porosity, even more so if they carry significant rock/ice mass fraction (*Jewitt and Sheppard,* 2002). Asteroid densities, calculated assuming they are equilibrium figures (*Sheppard and Jewitt,* 2002), are also plotted in Fig. 3 for five bodies that are probably rotationally deformed rubble piles (*Farinella et al.,* 1981). Asteroids are believed to have high refractory content, which explains why they have densities higher than

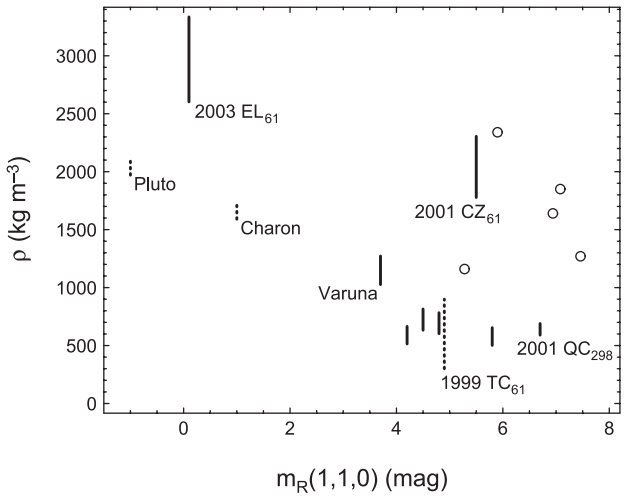

Fig. 3. Estimated density ranges as a function of absolute magnitude $m_R(1,1,0)$. Dashed lines correspond to densities of transneptunian binaries, estimated based on the satellite orbital properties. Solid lines indicate density ranges found for rotationally elongated TNOs assumed to be in hydrostatic equilibrium. Circles correspond to asteroids 15 Eunomia, 87 Sylvia, 16 Psyche, 107 Camilla, and 45 Eugenia, also thought to be rotationally elongated and in hydrostatic equilibrium (see *Sheppard and Jewitt,* 2002; *Farinella et al.,* 1981).

similar-sized TNOs. Furthermore, their densities are lower than that of solid rock, which also implies internal porosity (*Yeomans et al.,* 1997). Two TNOs, 2003 EL_{61} ($\rho \sim 2500$ kg m^{-3}) and 2001 CZ_{31} ($\rho \sim 2000$ kg m^{-3}), have rotational properties that require comparatively higher densities. Although this may be an indication of slightly higher rock/ice mass fractions or lower porosities in the case of these TNOs, the small numbers do not permit us to rule out any scenario. We note that substantial porosity may exist for even the largest icy TNOs if no significant heating has taken place in the body over the age of the solar system (*Durham et al.,* 2005). This may not be true for more rocky-type objects.

4.2. Spin Rate Versus Size

The number of TNOs with a well-measured spin period is about 40 as of July 2007 (Table 1). Besides being small, this sample is certainly biased. For instance, brighter objects with larger brightness variation are overrepresented, as are those with rotation periods P < 24 h. It is nevertheless interesting to compare the distribution of spin rates of TNOs with that of main-belt asteroids (MBAs). *Pravec et al.* (2003) presents a detailed study of asteroid rotation rates, using a sample of nearly 1000 lightcurves (*cfa-www.harvard.edu/iau/lists/LightcurveDat.html*). These lightcurves sample a range of sizes still mostly inaccessible in transneptunian studies, starting at bodies a few tens of meters in radius; only a few lightcurves have been reported for r ~ 10 km TNOs (*Trilling and Bernstein,* 2006) and Centaurs. Below we present a more indepth comparison between TNOs and MBAs. One TNO, 2003 EL_{61}, is outstanding in that it has the fastest rotation (P = 3.9154 ± 0.0002 h) measured for a solar system object larger than 100 km (*Rabinowitz et al.,* 2006).

Figure 4 shows the distributions of TNO and main-belt-asteroid spin periods. To minimize the effects of the aforementioned biases, only objects brighter than $m_R(1,1,0)$ = 6.5 mag, with at least Δm = 0.15 mag brightness variation range, and spinning faster than P = 20 h per full rotation were considered. In this range TNOs seem to spin slower, on average, than asteroids, with mean periods P_{TNO} = 8.4 h and P_{MBA} = 6.0 h (*Sheppard and Jewitt,* 2002; *Lacerda and Luu,* 2006). We used two nonparametric tests to test the null hypothesis that these samples are drawn from the same distribution, the Mann-Whitney U test and the Kolgomorov-Smirnov (K-S) test. The respective probabilities are 1.4% and 4.1%, which indicates that the parent distributions are likely different, but not unequivocally so. The different collisional environments as well as compositions within the main asteroid belt and Kuiper belt should account for any differences between the rotational distributions of the two populations. A similar plot of the TNOs and main-belt asteroids amplitude distributions shows no obvious differences (Fig. 5).

In Fig. 6 we plot spin period vs. absolute magnitude for the TNO data. To look for possible trends of spin rate with size, we follow *Pravec et al.* (2003) and plot a running mean

TABLE 1. Well-observed TNOs for variability.

Name			H* (mag)	Δm_R† (mag)	Single‡ (h)	Double§ (h)	Reference¶
(136199)	Eris	2003 UB_{313}¶	–1.2	<0.01	—	—	S
(134340)	Pluto¶		–1.0	0.33	153.2		B
(136472)		2005 FY_9	–0.4	<0.05	—	—	RST
(136108)		2003 EL_{61}¶	0.1	0.28 ± 0.04	—	3.9154 ± 0.0002	RB
(90377)	Sedna	2003 VB_{12}	1.6	0.02	10.273	—	G
(90482)	Orcus	2004 DW¶	2.3	0.04 ± 0.02	10.08 ± 0.01	—	OGS
				<0.03	—	—	S
(50000)	Quaoar	2002 LM_{60}¶	2.6	0.13 ± 0.03	—	17.6788 ± 0.0004	OG
(28978)	Ixion	2001 KX_{76}	3.2	<0.05	—	—	SS,OGC
(55565)		2002 AW_{197}	3.3	0.08 ± 0.07	8.86 ± 0.01	—	OGS
				<0.03	—	—	S
(55636)		2002 TX_{300}	3.3	0.08 ± 0.02	8.0 or 12.1	16.0 or 24.2	SS,OS
(55637)		2002 UX_{25}¶	3.6	<0.06	—	—	SS
				0.21 ± 0.06	7.2 or 8.4	—	RP
(20000)	Varuna	2000 WR_{106}	3.7	0.42 ± 0.03	—	6.34 ± 0.01	JS,OGC
		2003 AZ_{84}	3.9	0.12 ± 0.02	6.72	13.44	SS,OGS
(90568)		2004 GV_9	4.0	<0.08	—	—	S
(42301)		2001 UR_{163}	4.2	<0.08	—	—	SS
(84922)		2003 VS_2	4.2	0.21 ± 0.02	—	7.41	S,OGS
(19308)		1996 TO_{66}	4.5	0.25 ± 0.05	5.9	11.8	OH,SS,BO,SB
(120348)		2004 TY_{364}	4.5	0.22 ± 0.02	5.85 ± 0.01	11.70 ± 0.01	S
		2001 QF_{298}	4.7	<0.12	—	—	SS
(26375)		1999 DE_9	4.7	<0.10	>12?	—	SJ
(38628)	Huya	2000 EB_{173}	4.7	<0.06	—	—	SJ,SR,OGC,LL
(24835)		1995 SM_{55}	4.8	0.19 ± 0.05	4.04 ± 0.03	8.08 ± 0.03	SS
(19521)	Chaos	1998 WH_{24}	4.9	<0.10	—	—	SJ,LL
(47171)		1999 TC_{36}¶	4.9	<0.05	—	—	SS,OGC,LL
(82075)		2000 YW_{134}	5.0	<0.1	—	—	SS
(120132)		2003 FY_{128}	5.0	<0.08	—	—	S
(79360)		1997 CS_{29}	5.1	<0.08	—	—	SJ
(119979)		2002 WC_{19}¶	5.1	<0.05	—	—	S
(26181)		1996 GQ_{21}	5.2	<0.10	—	—	SJ
(55638)		2002 VE_{95}	5.3	<0.06	—	—	SS
				0.08 ± 0.04	6.76,7.36,9.47	—	OGS
(126154)		2001 YH_{140}	5.4	0.21 ± 0.04	13.25 ± 0.2	—	S,OGS
(15874)		1996 TL_{66}	5.4	<0.12	—	—	RT,LJ,OGS
(148780)		2001 UQ_{18}	5.4	<0.3	—	—	S
(88611)		2001 QT_{297} 1¶	5.5	<0.1	—	—	OKE
		2001 QT_{297} 2¶		0.6	4.75	—	OKE
(150642)		2001 CZ_{31}	5.7	<0.20	—	—	SJ
				0.21 ± 0.02	4.71	—	LL
		2001 KD_{77}	5.8	<0.07	—	—	SS
(26308)		1998 SM_{165}**	5.8	0.45	7.1		R,SS
(40314)		1999 KR_{16}	5.8	0.18 ± 0.04	5.840 or 5.929	11.680 or 11.858	SJ
(35671)		1998 SN_{165}	5.8	0.16 ± 0.01	8.84	—	LL
(66652)		1999 RZ_{253}	5.9	<0.05	—	—	LL
(47932)		2000 GN_{171}	6.0	0.61 ± 0.03	—	8.329 ± 0.005	SJ
(82158)		2001 FP_{185}	6.1	<0.06	—	—	SS
(79983)		1999 DF_9	6.1	0.40 ± 0.02	6.65	—	LL
(82155)		2001 FZ_{173}	6.2	<0.06	—	—	SJ
(80806)		2000 CM_{105}	6.2	<0.14	—	—	LL
		2003 QY_{90} 1¶	6.3	0.34 ± 0.12	3.4 ± 1.1	—	KE
		2003 QY_{90} 2¶		0.90 ± 0.36	7.1 ± 2.9	—	KE
		1996 TS_{66}	6.4	<0.15	—	—	LL
(33340)		1998 VG_{44}	6.5	<0.10	—	—	SJ
(139775)		2001 QG_{298}	6.7	1.14 ± 0.04	—	13.7744 ± 0.0004	SSJ
(15875)		1996 TP_{66}	6.8	<0.15	—	—	RT,CB
(15789)		1993 SC	6.9	<0.15	—	—	RT,D
(15820)		1994 TB	7.1	<0.15	—	—	SS
(33128)		1998 BU_{48}	7.2	0.68 ± 0.04	4.9 or 6.3	9.8 or 12.6	SJ

TABLE 1. (continued).

Name			H* (mag)	Δm_R† (mag)	Single‡ (h)	Double§ (h)	Reference¶
(42355)	Typhon	2002 CR_{46}¶	7.2	<0.05	—	—	SS,OGC
		1997 CV_{29}	7.4	0.4	—	16	CK
(32929)		1995 QY_9	7.5	0.60	7.3	—	RT,SS
(91133)		1998 HK_{151}	7.6	<0.15	—	—	SS
		2000 FV_{53}	8.2	0.07	3.79 or 7.5	—	TB
		2003 BG_{91}	10.7	0.18	4.2	—	TB
		2003 BF_{91}	11.7	1.09	7.3 or 9.1	—	TB
		2003 BH_{91}	11.9	0.42	?	—	TB
Centaurs							
(10199)	Chariklo	1997 CU26	6.4	?	?	?	PLO
(2060)	Chiron	1977 UB**	6.5	0.09 to 0.45	—	5.917813	BBH,L,MB
(5145)	Pholus	1992 AD	7.0	0.15 to 0.6	—	9.98	BB,H,F,TRC
(54598)	Bienor	2000 QC_{243}	7.6	0.75 ± 0.09	4.57 ± 0.02	—	OBG
(29981)		1999 TD_{10}	8.8	0.65 ± 0.05	7.71 ± 0.02	—	OGC,RPP,MH
(73480)		2002 PN_{34}	8.2	0.18 ± 0.04	4.23 or 5.11	—	OGC
(120061)		2003 CO_1	8.9	0.10 ± 0.05	4.99	—	OGS
(8405)	Asbolus	1995 GO	9.0	0.55		8.93	BL,DN
(32532)	Thereus	2001 PT_{13}	9.0	0.16 ± 0.02	4.1546 ± 0.0001	—	OBG
(83982)	Crantor	2002 GO_9	9.1	0.14 ± 0.04	6.97 or 9.67	—	OGC
(60558)		2000 EC_{98}	9.5	0.24 ± 0.06	13.401	—	RP
(31824)	Elatus	1999 UG_5	10.1	0.102 to 0.24	13.25 or 13.41	—	BM,GO
(52872)	Okyrhoe	1998 SG_{35}	11.3	0.2	8.3	—	BMF

*Absolute magnitude of the object.

†The peak to peak range of the lightcurve.

‡The lightcurve period if there is one maximum per period. If not shown the uncertainties are at the last significant digit.

§The lightcurve period if there is two maximum per period. If not shown the uncertainties are at the last significant digit.

¶A known binary TNO with both components lightcurves 1 and 2 known if labeled.

**Centaurs observed to have coma.

References: BBH = *Bus et al.* (1989); L = *Luu and Jewitt* (1990); BB = *Buie and Bus* (1992); H = *Hoffmann et al.* (1993); MB = *Marcialis and Buratti* (1993); BL = *Brown and Luu* (1997); B = *Buie et al.* (1997); D = *Davies et al.* (1997); DN = *Davies et al.* (1998); LJ = *Luu and Jewitt* (1998); CB = *Collander-Brown et al.* (1999); RT = *Romanishin and Tegler* (1999); OH = *Hainaut et al.* (2000); F = *Farnham* (2001); GO = *Gutierrez et al.* (2001); R = *Romanishin et al.* (2001); PLO = *Peixinho et al.* (2001); JS = *Jewitt and Sheppard* (2002); SJ = *Sheppard and Jewitt* (2002); SR = *Schaefer and Rabinowitz* (2002); BM = *Bauer et al.* (2002); OBG = *Ortiz et al.* (2002); SB = *Sekiguchi et al.* (2002); SS = *Sheppard and Jewitt* (2003); OGC = *Ortiz et al.* (2003a); OG = *Ortiz et al.* (2003b); OKE = *Osip et al.* (2003); BMF = *Bauer et al.* (2003); RPP = *Rousselot et al.* (2003); SSJ = *Sheppard and Jewitt* (2004); OS = *Ortiz et al.* (2004); CK = *Chorney and Kavelaars* (2004); MH = *Mueller et al.* (2004); G = *Gaudi et al.* (2005); TRC = *Tegler et al.* (2005); TB = *Trilling and Bernstein* (2006); RP = *Rousselot et al.* (2005b); OGS = *Ortiz et al.* (2006); RB = *Rabinowitz et al.* (2006); LL = *Lacerda and Luu* (2006); KE = *Kern and Elliot* (2006); BO = *Belskaya et al.* (2006); RST = *Rabinowitz et al.* (2007); S = *Sheppard* (2007).

of sets of four consecutive data points (jagged solid line). We also plot a running median for the same box size (jagged dashed line). Although the data may seem very scattered, the running mean hints at a trend of smaller TNOs spinning slightly faster. To test this hypothesis we employ the runs test for randomness (*Wall and Jenkins,* 2003), using as binary statistic the position of the measured periods relative to the median of all the measurements: Each measurement is either above or below the median, with probability 1/2. This test determines if successive (sorted by object absolute magnitude) spin period measurements are independent by checking if the number of runs (sequences of periods above and below the median) is sufficiently close to the expected value given the sample size. For the data plotted in Fig. 6, 11.52 ± 2.40 runs are expected and 12 are found. The data are thus perfectly consistent with consecutive measurements being independent.

4.3. Amplitude Versus Size

The available TNO lightcurve ranges (Δm) are plotted vs. object absolute magnitude in Fig. 7. The data suggest aslight tendency of higher variability for smaller TNOs. Except for the high-angular momentum TNOs 2003 EL_{61} and (20000) Varuna, all other objects intrinsically brighter than $m_R(1,1,0) \sim 6.0$ mag ($r \sim 110$ km assuming a 10% albedo) have relatively low variability ($\Delta m \lesssim 0.25$ mag). The same is not true for smaller (fainter) TNOs for which a much larger spread in lightcurve range exists. We used both the Mann-Whitney and K-S tests to find the absolute magni-

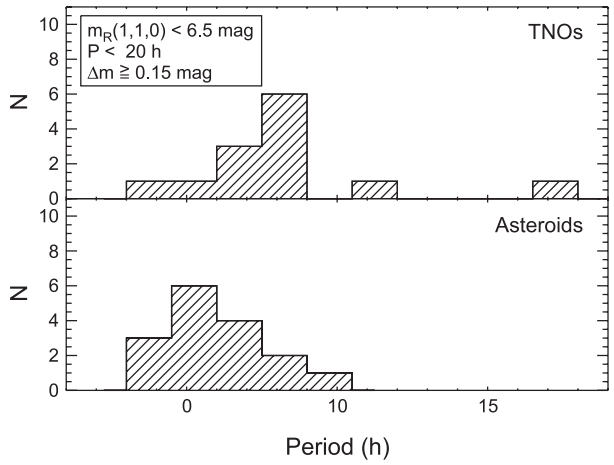

Fig. 4. Histogram of spin period for TNOs and asteroids. To minimize biases, only objects brighter than $m_R(1,1,0) = 6.5$ mag, spinning faster than P = 20 h, and with lightcurve ranges larger than Δm = 0.15 mag have been considered. As discussed in the text, the TNOs have statistically longer periods ($\bar{P}_{TNO} \sim 8.4$ h) than the main-belt asteroids ($\bar{P}_{MBA} \sim 6.0$ h) of similar size.

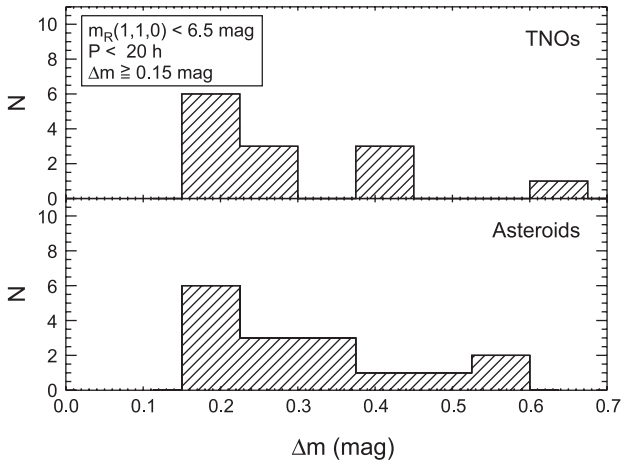

Fig. 5. Histogram of lightcurve range Δm for TNOs and asteroids. To minimize biases, only objects brighter than $m_R(1,1,0) = 6.5$ mag, spinning faster than P = 20 h, and with lightcurve ranges larger than Δm = 0.15 mag have been considered.

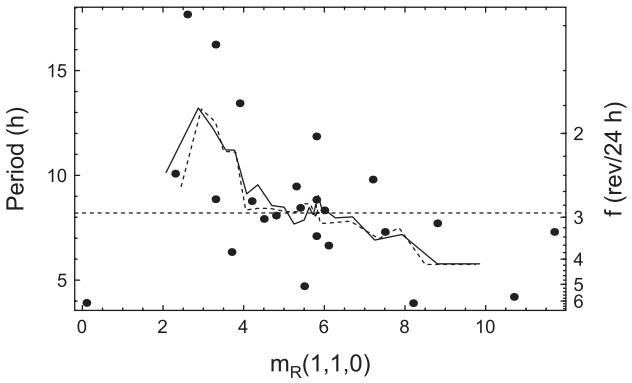

Fig. 6. Absolute magnitude vs. spin periods of the TNOs with well-measured lightcurves. As explained in the text, it appears that smaller TNOs may spin slightly faster than the larger TNOs. Pluto has not been plotted.

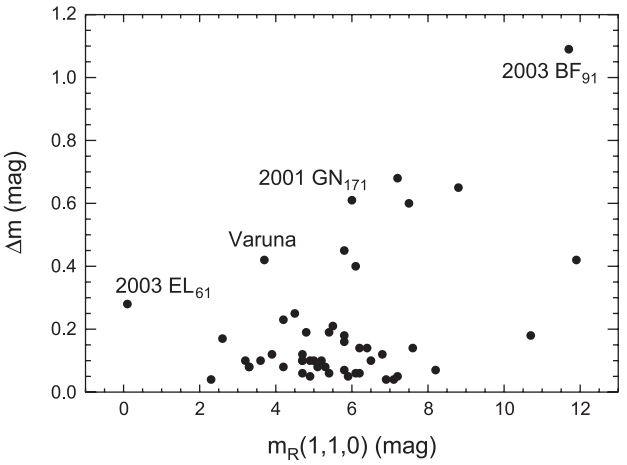

Fig. 7. Total lightcurve range plotted as a function of absolute magnitude for some of the TNOs showing rotational lightcurves in Table 1. High specific angular momentum TNOs 2003 EL_{61}, (20000) Varuna, 2001 GN_{171}, and 2003 BF_{91} are labeled. The likely contact binary, 2001 QG_{298}, has not been plotted. A statistically obvious trend of smaller TNOs having larger-amplitude lightcurves can be seen.

tude boundary that maximizes the difference in the peak-to-peak amplitude distributions of larger and smaller objects. We split TNOs at values of absolute magnitude from 3.0 to 8.5 in steps of 0.5, and calculated the probabilities $p_{U\text{-}test}$ and $p_{K\text{-}S}$ that the two populations were drawn from the same parent distribution. Both tests indicate $m_R(1,1,0) = 5.5$ (r ~ 150 km assuming 10% albedo) as maximum difference boundary, with $p_{U\text{-}test} = 0.16$ and $p_{K\text{-}S} = 0.19$. Choosing $m_R(1,1,0) = 6.5$ (r ~ 90 km assuming 10% albedo) yields comparable probabilities, $p_{U\text{-}test} = 0.17$ and $p_{K\text{-}S} = 0.20$. In conclusion, the data suggest that smaller TNOs could have larger lightcurve variability. This appears consistent with the idea that the smaller objects are more irregular in shape and collisionally evolved.

5. SHAPE DISTRIBUTION OF TRANSNEPTUNIAN OBJECTS

Due to their minute angular size, the shapes of most individual TNOs cannot be measured directly. However, under the assumption that the periodic brightness variations in a TNO lightcurve are caused by the object's nonspherical

shape, we can statistically investigate the TNO shape distribution from the distribution of lightcurve peak-to-peak amplitudes (*Sheppard and Jewitt,* 2002, *Lacerda and Luu,* 2003, *Luu and Lacerda,* 2003). In simple terms, a population of elongated objects will typically produce large brightness variations, whereas a population of nearly spherical objects will predominantly cause nearly flat lightcurves.

As a simplification we will consider TNOs to be prolate ellipsoids with semiaxis $a > b = c$ and use $\tilde{a}$ to represent the shape of a given TNO. The shape distribution can be approximated by function $f(\tilde{a})$, which when multiplied by the element $d\tilde{a}$ gives the probability of finding a TNO with axis-ratio between $\tilde{a}$ and $\tilde{a} + d\tilde{a}$. As mentioned in section 3.2, the aspect angle θ, defined as the smallest angular distance between the line of sight and the TNO's spin axis, also influences the range of brightness variation. Since the distribution of spin orientations of TNOs is unknown, the most reasonable *a priori* assumption is that the orientations are random. Using these presumptions, Lacerda and Luu (2003) have shown that if TNOs have a shape distribution $f(\tilde{a})$ then the probability of finding a TNO with a lightcurve range $\Delta m \geq 0.15$ mag is given by

$$p(\Delta m \geq 0.15) \approx \int_{\sqrt{K}}^{\infty} f(\tilde{a}) \sqrt{\frac{\tilde{a}^2 - K}{(\tilde{a}^2 - 1)K}}\, d\tilde{a} \qquad (8)$$

where $\sqrt{K} = 10^{0.4 \times 0.15}$ is the axis ratio $\tilde{a}$ at which $\Delta m = 0.15$ mag for an object viewed equatorially (see *Lacerda and Luu,* 2003). This equation can be used to constrain the shape distribution $f(\tilde{a})$.

The best estimate of $p(\Delta m \geq 0.15)$ is the fraction of TNOs that show brightness variations larger than 0.15 mag. From Table 1 we see that about 38% of the listed TNOs have lightcurve ranges $\Delta m \geq 0.15$ mag. Following previous authors, we adopt $\Delta m = 0.15$ mag as a threshold for variability detection because most ranges below this value are uncertain and usually taken as upper limits. Table 1 also shows that there is a significant fraction of objects with large peak-to-peak brightness variations: 16% have $\Delta m > 0.40$ mag. These observational constraints seem to indicate that any candidate shape distribution must allow a large fraction of nearly round objects, but also a significant amount of very elongated objects. A power-law type distribution of the form $f(\tilde{a}) \propto \tilde{a}^{-q}$ has been shown to fit best the available data (*Sheppard and Jewitt,* 2002; *Luu and Lacerda,* 2003). The best-fit slope, calculated using the method described in *Lacerda and Luu* (2003) and the data from Table 1, is $q = 4.8^{+1.2}_{-1.0}$.

More recently it has been shown that larger and smaller TNOs may have different shape distributions (*Lacerda and Luu,* 2006). This is to be expected because the material strength in smaller TNOs is likely sufficient to maintain irregular shapes, while the larger TNOs should have rounder shapes as a result of their gravity. Figure 7 shows lightcurve ranges plotted against absolute magnitude for the TNOs in Table 1. Albedo measurements exist only for a few of the listed objects. For this reason we choose to sort these TNOs by absolute magnitude, as proxy for size. We place the line between *larger* and *smaller* TNOs at $m_R(1,1,0) = 5.5$ mag. Assuming a 0.10 (0.04) albedo, this corresponds to about 360 km (570 km) diameter. If we apply the procedure described above to TNOs brighter and fainter than 5.5 mag separately, we find that the power-law shape distributions that best fit each of the two groups are considerably different: for larger ($m_R(1,1,0) \leq 5.5$ mag) TNOs we find $q = 6.0^{+2.2}_{-1.7}$, while for smaller objects the best slope is $q = 3.8^{+1.6}_{-1.3}$. Although the significance is low (~1.5σ), the data indeed show the trend of more elongated (or irregular) shapes for smaller objects.

Inspection of Fig. 7 suggests that a simple relation between size and shape may not exist, because the latter will certainly depend on other factors such as the collisional history of individual objects. The cluster of objects with $\Delta m \leq 0.3$ mag variability may have had a milder collisional evolution than larger specific angular momentum TNOs such as (136108) 2003 EL_{61}, (20000) Varuna, (47932) 2000 GN_{171}, and 2003 BF_{91}.

6. ANGULAR MOMENTUM OF TRANSNEPTUNIAN OBJECTS

The extremely fast rotations observed for several large TNOs [e.g., (20000) Varuna and (136108) 2003 EL_{61}] as well as relatively small satellites that are known around large TNOs [such as Pluto, 2003 EL_{61}, and Eris (2003 UB_{313}); see chapter by Noll et al.] show that many of the Kuiper belt objects (KBOs) have high amounts of specific angular momentum (Fig. 2). It is probably safe to assume this high angular momentum was imparted through collisions. In the current Kuiper belt the collision timescale to significantly modify the angular momentum of the largest TNOs is about 10^{12} yr (*Jewitt and Sheppard,* 2002). Thus the collisions likely occurred in an earlier Kuiper belt that had over 100× more large KBOs than we see there today.

The likely outcome of a large collision on a self-gravitating body is a fractured, rubble-pile-type structure (*Asphaug et al.,* 1998). Once formed, rubble-pile structures can insulate the object from disruption from further collisions by absorbing the energy of impact efficiently. In addition, the porous ices probably found in KBOs may be efficient at dissipating impact energy (*Arakawa et al.,* 2002; *Giblin et al.,* 2004). The true outcome of an impact depends on several parameters including the size of the impactor, target, and angle of impact. A glancing low-velocity collision will substantially alter the spin of a target body and may create some of the satellites and fast-spinning KBOs (*Leinhardt et al.,* 2000; *Durda et al.,* 2004).

7. CORRELATIONS WITH ROTATIONAL CHARACTERISTICS

It seems plausible that the evolutionary path that resulted in an object having a specific orbit might have affected the rotation state of that particular object. Therefore, the study of rotational properties as a function of orbital and other physical parameters might yield useful information concerning evolutionary paths. A similar reasoning has been fol-

TABLE 2. Correlation (>95%) of rotational characteristics with physical and orbital parameters.

Param*	Spear ρ†	Error	Sig (%)‡	N§
Δm vs. H	0.335	0.005	99.45	73
Δm vs. Q	–0.292	0.016	97.12	58
Δm vs. e	–0.279	0.022	96.19	58
Δm vs. H	0.285	0.026	96.13	58
P vs. i	0.614	0.034	95.98	13
Δm vs. Q	–0.240	0.044	95.48	73
P vs. H	–0.347	0.055	94.99	36

*Orbital parameters where Δm is the lightcurve amplitude, H is absolute magnitude, Q is aphelion distance, e is eccentricity, P is the rotation period, and i is inclination of the orbit.

†Spearman.

‡Significance level.

§Number of objects used. 73 means all TNOs and Centaurs used in the correlation, 58 means only the TNOs were used, 36 means only TNOs with well-measured lightcurves used, and 13 means only Plutinos were used.

lowed for colors (see chapter by Doressoundiram et al.). Unfortunately, the number of TNOs whose photometric variability has been measured is small, but the sample size is now large enough to start some analysis. *Santos-Sanz et al.* (2006) studied possible correlations of rotation periods, P, and amplitudes, Δm, vs. orbital and physical parameters using 73 TNOs and Centaurs; this includes the 30 or so with determined periods and amplitudes as well as the more numerous objects that have been well observed but have no detectable variability (see Table 1).

The strongest significant correlation found (>99%) was discussed in section 4.3, in which the rotational amplitude is correlated with the absolute magnitude (size) of the object. A few weaker and less evident correlations were found (>95%) but more data are needed to confirm them as significant (see Table 2). The next highest correlation is that of the amplitude vs. aphelion distance, Q (in this case anticorrelation), which is difficult to explain in terms of plausible physical processes that would decrease the amplitude of the lightcurve (and presumably the degree of irregularity) for the objects with larger aphelion distances. Maybe objects further out collide less often or sublimate less material over the age of the solar system.

Binary objects may also affect these statistics since any satellite (which maybe unknown) may influence the rotation, although in most cases any companions are expected to have negligible effects. It may also be interesting to analyze the large and small bodies separately as both families have clearly different photometric amplitudes but the current sample size is too small.

8. CONCLUDING REMARKS

Our knowledge on the rotational information of the largest TNOs is still a work in progress. The recent discovery of several large TNOs has shown that the lightcurve measurements of such objects are still in their infancy. Future lightcurve measurements of large objects are highly desirable using small- and medium-class telescopes. Once we increase the lightcurve inventory and their time bases to decades, we will start to be able to determine the pole orientations of TNOs.

To date there is little or no information about the rotations of small TNOs (r < 50 km). Future observations of these TNOs would be beneficial to determine if their rotation periods and amplitudes are similar to the larger objects observed to date. A transition between gravitational to mechanical structural domination should be observed for objects with radii between 50 and 100 km. The smaller objects (r < 50 km) should show a significantly different distribution of rotation periods and amplitudes than the larger objects (r > 100 km). TNOs with radii smaller than about 50 km are probably just collisional shards with shapes and rotations presumably set by the partitioning of kinetic energy delivered by the projectile responsible for breakup. Unlike the larger TNOs their rotation states are much more influenced from recent collisional events. These smaller TNOs would be much fainter than the larger objects and thus would require a number of nights on large-class telescopes (6–10 m) to obtain the signal-to-noise needed to detect their lightcurves.

In addition, it would be beneficial to obtain lightcurve information on the binary TNOs to determine their angular momentum and orbital rotational states.

Acknowledgments. We thank P. Santos-Sanz for sharing results prior to publication. S.S.S. was supported for this work by NASA through Hubble Fellowship grant #HF-01178.01-A awarded by the Space Telescope Science Institute, which is operated by the Association of Universities for Research in Astronomy, Inc., for NASA, under contract NAS 5-26555. P.L. is grateful to Fundação para a Ciência e a Tecnologia (BPD/SPFH/18828/2004) for financial support. J.L.O. acknowledges support from AYA-2005-07808-C01-03.

REFERENCES

Arakawa M., Leliwa-Kopystynski J., and Maeno N. (2002) Impact experiments on porous icy-silicate cylindrical blocks and the implication for disruption and accumulation of small icy bodies. *Icarus, 158,* 516–531.

Asphaug D. and Benz W. (1996) Size, density, and structure of Comet Shoemaker-Levy 9 inferred from the physics of tidal breakup. *Icarus, 121,* 225–248.

Asphaug D., Ostro S., Hudson R., Scheeres D., and Benz W. (1998) Disruption of kilometre-sized asteroids by energetic collisions. *Nature, 393,* 437.

Bauer J., Meech K., Fernandez Y., Farnham T., and Roush T. (2002) Observations of the Centaur 1999 UG5: Evidence of a unique outer solar system surface. *Publ. Astron. Soc. Pac., 114,* 1309–1321.

Bauer J., Meech K., Fernandez Y., Pittichova J., Hainaut O., Boehnhardt H., and Delsanti A. (2003) Physical survey of 24 Centaurs with visible photometry. *Icarus, 166,* 195–211.

Belskaya I., Ortiz J., Rousselot P., Ivanova V., Vorisov G., Shevchenko V., and Peixinho N. (2006) Low phase angle effects in photometry of trans-neptunian objects: 20000 Varuna and 19308 (1996 TO_{66}). *Icarus, 184,* 277–284.

Belton J. and Gandhi A. (1988) Application of the CLEAN algorithm to cometary light curves. *Bull. Am. Astron. Soc., 20,* 836.

Bernstein G., Trilling D., Allen R., Brown M., Holman M., and Malhotra R. (2004) The size distribution of trans-Neptunian bodies. *Astron. J., 128,* 1364–1390.

Binzel R., Farinella P., Zappala V., and Cellino A. (1989) Asteroid rotation rates: Distributions and statistics. In *Asteroids II* (R. P. Binzel et al., eds.), pp. 415–441. Univ. of Arizona, Tucson.

Brown W. and Luu J. (1997) CCD photometry of the Centaur 1995 GO. *Icarus, 126,* 218–224.

Buie M. and Bus S. (1992) Physical observations of (5145) Pholus. *Icarus, 100,* 288–294.

Buie M., Tholen D., and Wasserman L. (1997) Separate lightcurves of Pluto and Charon. *Icarus, 125,* 233–244.

Burns J. and Safronov V. (1973) Asteroid nutation angles. *Mon. Not. R. Astron. Soc., 165,* 403–411.

Bus S., Bowell E., Harris A., and Hewitt A. (1989) 2060 Chiron — CCD and electronographic photometry. *Icarus, 77,* 223–238.

Capaccioni F., Cerroni P., Coradini M., Farinella P., Flamini E., et al. (1984) Shapes of asteroids compared with fragments from hypervelocity impact experiments. *Nature, 308,* 832–834.

Catullo V., Zappala V., Farinella P., and Paolicchi P. (1984) Analysis of the shape distribution of asteroids. *Astron. Astrophys., 138,* 464–468.

Chandrasekhar S. (1969) *Ellipsoidal Figures of Equilibrium*. Yale Univ., New Haven.

Chorney N. and Kavelaars J. (2004) A rotational light curve for the Kuiper belt object 1997 CV29. *Icarus, 167,* 220–224.

Collander-Brown S., Fitzsimmons A., Fletcher E., Irwin M., and Williams I. (1999) Light curves of the trans-Neptunian objects 1996 TP66 and 1994 VK8. *Mon. Not. R. Astron. Soc., 308,* 588–592.

Davies J., McBride N., and Green S. (1997) Optical and infrared photometry of Kuiper belt object 1993SC. *Icarus, 125,* 61–66.

Davies J., McBride N., Ellison S., Green S., and Ballantyne D. (1998) Visible and infrared photometry of six Centaurs. *Icarus, 134,* 213–227.

Davis D. and Farinella P. (1997) Collisional evolution of Edgeworth-Kuiper belt objects. *Icarus, 125,* 50–60.

Degewij J., Tedesco E., and Zellner B. (1979) Albedo and color contrasts on asteroid surfaces. *Icarus, 40,* 364–374.

Duncan M., Quinn T., and Tremaine S. (1988) The origin of short-period comets. *Astrophys. J. Lett., 328,* L69–L73.

Durda D., Bottke W., Enke B., Merline W., Asphaug E., Richardson D., and Leinhardt Z. (2004) The formation of asteroid satellites in large impacts: Results from numerical simulations. *Icarus, 170,* 243–257.

Durham W., McKinnon W., and Stern L. (2005) Cold compaction of water ice. *Geophys. Res. Lett., 32,* L18202.

Dworetsky M. (1983) A period-finding method for sparse randomly spaced observations, or How long is a piece of string? *Mon. Not. R. Astron. Soc., 203,* 917–924.

Farinella P. (1987) Small satellites. In *The Evolution of the Small Bodies of the Solar System* (M. Fulchignoni and L. Kresak, eds.), p. 276. North-Holland, Amsterdam.

Farinella P. and Davis D. (1996) Short-period comets: Primordial bodies or collisional fragments? *Science, 273,* 938–941.

Farinella P. and Zappala V. (1997) The shapes of the asteroids. *Adv. Space Res., 19,* 181–186.

Farinella P., Paolicchi P., Tedesco E., and Zappala V. (1981) Triaxial equilibrium ellipsoids among the asteroids. *Icarus, 46,* 114–123.

Farnham T. (2001) The rotation axis of Centaur 5145 Pholus. *Icarus, 152,* 238–245.

Fernandez J. A. (1980) On the existence of a comet belt beyond Neptune. *Mon. Not. R. Astron. Soc., 192,* 481–491.

Fujiwara A., Kamimoto G., and Tsukamoto A. (1978) Expected shape distribution of asteroids obtained from laboratory impact experiments. *Nature, 272,* 602–603.

Gaudi B. S., Stanek K. Z., Hartman J. D., Holman, M. J., and McLeod B. A. (2005) On the rotation period of (90377) Sedna. *Astrophys. J., 629,* L49–L52.

Giblin I., Davis D., and Ryan E. (2004) On the collisional disruption of porous icy targets simulating Kuiper belt objects. *Icarus, 171,* 487–505.

Gutierrez P., Oritz J., Alexandrino E., Roos-Serote M., and Doressoundiram A. (2001) Short term variability of Centaur 1999 UG5. *Astron. Astrophys., 371,* L1–L4.

Hainaut O., Delahodde C., Boehnhardt H., Dott E., Barucci M. A., et al. (2000) Physical properties of TNO 1996 TO66. Lightcurves and possible cometary activity. *Astron. Astrophys., 356,* 1076–1088.

Harris A. (1994) Tumbling asteroids. *Icarus, 107,* 209–211.

Harris A., Young J., Bowell E., Martin L., Millis R., Poutanen M., Scaltriti F., Zappala V., Schober H., Debehogne H., and Zeigler K. (1989) Photoelectric observations of asteroids 3, 24, 60, 261, and 863. *Icarus, 77,* 171–186.

Hartmann W. and Cruikshank D. (1978) The nature of Trojan asteroid 624 Hektor. *Icarus, 36,* 353–366.

Hestroffer D., Marchis F., Fusco T., and Berthier J. (2002) Adaptive optics observations of asteroid (216) Kleopatra. *Astron. Astrophys., 394,* 339–343.

Hoffmann M., Fink U., Grundy W., and Hicks M. (1993) Photometric and spectroscopic observations of 5145 Pholus. *J. Geophys. Res., 98,* 7403–7407.

Holsapple K. (2001) Equilibrium configurations of solid cohesionless bodies. *Icarus, 154,* 432–448.

Holsapple K. (2004) Equilibrium figures of spinning bodies with self-gravity. *Icarus, 172,* 272–303.

Jeans J. (1919) *Problems of Cosmogony and Stellar Dynamics*. Cambridge Univ., London/New York.

Jewitt D. and Sheppard S. (2002) Physical properties of trans-Neptunian object (20000) Varuna. *Astron. J., 123,* 2110–2120.

Kern S. and Elliot J. (2006) Discovery and characteristics of the Kuiper belt binary 2003QY90. *Icarus, 183,* 179–185.

Lacerda P. and Luu J. (2003) On the detectability of lightcurves of Kuiper belt objects. *Icarus, 161,* 174–180.

Lacerda P. and Luu J. (2006) Analysis of the rotational properties of Kuiper Belt objects. *Astron. J., 131,* 2314–2326.

Leinhardt Z., Richardson D., and Quinn T. (2000) Direct N-body simulations of rubble pile collisions. *Icarus, 146,* 133–151.

Leone G., Farinella P., Paolicchi P., and Zappala V. (1984) Equilibrium models of binary asteroids. *Astron. Astrophys., 140,* 265–272.

Lomb N. (1976) Least-squares frequency analysis of unequally spaced data. *Astrophys. Space Sci., 39,* 447–462.

Luu J. and Jewitt D. (1990) Cometary activity in 2060 Chiron. *Astron. J., 100,* 913–932.

Luu J. and Jewitt D. (1998) Optical and infrared reflectance spectrum of Kuiper belt object 1996 TL66. *Astrophys. J., 494,* L117–L120.

Luu J. and Lacerda P. (2003) The shape distribution of Kuiper belt objects. *Earth Moon Planets, 92,* 221–232.

Magnusson P. (1991) Analysis of asteroid lightcurves. III — Albedo variegation. *Astron. Astrophys., 243,* 512–520.

Marcialis R. and Buratti B. (1993) CCD photometry of 2060 Chiron in 1985 and 1991. *Icarus, 104,* 234–243.

Mueller B., Hergenrother C., Samarasinha N., Campins H., and McCarthy D. (2004) Simultaneous visible and near-infrared time resolved observations of the outer solar system object (29981) 1999 TD10. *Icarus, 171,* 506–515.

Ortiz J., Baumont S., Gutierrez P., and Roos-Serote M. (2002) Lightcurves of Centaurs 2000 QC243 and 2001 PT13. *Astron. Astrophys., 388,* 661–666.

Ortiz J., Gutierrez P., Casanova V., and Sota A. (2003a) A study of short term variability in TNOs and Centaurs from Sierra Nevada observatory. *Astron. Astrophys., 407,* 1149–1155.

Ortiz J., Gutierrez P., Sota A., Casanova V., and Teixeira V. (2003b) Rotational brightness variations in trans-Neptunian object 50000 Quaoar. *Astron. Astrophys., 409,* L13–L16.

Ortiz J., Sota A., Moreno R., Lellouch E., Biver N., et al. (2004) A study of trans-Neptunian object 55636 (2002 TX300). *Astron. Astrophys., 420,* 383–388.

Ortiz J., Gutierrez P., Santos-Sanz P., Casanova V., and Sota A. (2006) Short-term rotational variability of eight KBOs from Sierra Nevada observatory. *Astron. Astrophys., 447,* 1131–1144.

Osip D., Kern S., and Elliot J. (2003) Physical characterization of the binary Edgeworth-Kuiper belt object 2001 QT297. *Earth Moon Planets, 92,* 409–421.

Ostro S., Hudson R. S., Nolan M. C., Margot J.-L., Scheeres D. J., et al. (2000) Radar observations of asteroid 216 Kleopatra. *Science, 288,* 836–839.

Pravec P., Harris A., and Michalowski T. (2003) Asteroid rotations. In *Asteroids III* (W. F. Bottke Jr. et al., eds.), pp. 113–122. Univ. of Arizona, Tucson.

Peixinho N., Lacerda P., Ortiz J., Doressoundiram A., Roos-Serote M., and Gutiérrez P. (2001) Photometric study of Centaurs 10199 Chariklo (1997 CU_{26}) and 1999 UG_5. *Astron. Astrophys., 371,* 753–759.

Rabinowitz D., Barkume K., Brown M., Roe H., Schwartz M., et al. (2006) Photometric observations constraining the size, shape and albedo of 2003 EL61, a rapidly rotating, Pluto-sized object in the Kuiper belt. *Astrophys. J., 639,* 1238–1251.

Rabinowitz D., Schaefer B., and Tourtellote S. (2007) The diverse solar phase curves of distant icy bodies. Part 1: Photometric observations of 18 trans-Neptunian objects, 7 Centaurs, and Nereid. *Astron. J., 133,* 26–43.

Romanishin W. and Tegler S. (1999) Rotation rates of Kuiper-belt objects from their light curves. *Nature, 398,* 129–132.

Romanishin W., Tegler S., Rettig T., Consolmagno G., and Botthof B. (2001) *Proc. Natl. Acad. Sci., 98,* 11863.

Rousselot P., Petit J., Poulet F., Lacerda P., and Ortiz J. (2003) *Astron. Astrophys., 407,* 1139–1147.

Rousselot P., Petit J., and Belskaya I. (2005a) Besancon photometric database for Kuiper-belt objects and Centaurs. Abstract presented at Asteroids, Comets, Meteors 2005, August 7–12, 2005, Rio de Janeiro, Brazil.

Rousselot P., Petit J., Poulet F., and Sergeev A. (2005b) Photometric study of Centaur (60558) 2000 EC98 and trans-Neptunian object (55637) 2002 UX25 at different phase angles. *Icarus, 176,* 478–491.

Scargle J. D. (1982) Studies in astronomical time series analysis. II — Statistical aspects of spectral analysis of unevenly spaced data. *Astrophys. J., 263,* 835–853.

Schaefer B. and Rabinowitz D. (2002) Photometric light curve for the Kuiper belt object 2000 EB173 on 78 nights. *Icarus, 160,* 52–58.

Santos-Sanz P., Ortiz J., and Gutiérrez P. (2006) Rotational properties of TNOs and Centaurs. Abstract presented at the International Workshop on Trans-Neptunian Objects: Dynamical and Physical Properties, July 3–7, 2006, Catania, Italy.

Sekiguchi T., Boehnhardt H., Hainaut O., and Delahodde C. (2002) Bicolour lightcurve of TNO 1996 TO66 with the ESO-VLT. *Astron. Astrophys., 385,* 281–288.

Sheppard S. and Jewitt D. (2002) Time-resolved photometry of Kuiper belt objects: Rotations, shapes, and phase functions. *Astron. J., 124,* 1757–1775.

Sheppard S. and Jewitt D. (2003) Hawaii Kuiper belt variability project: An update. *Earth Moon Planets, 92,* 207–219.

Sheppard S. and Jewitt D. (2004) Extreme Kuiper belt object 2001 QG298 and the fraction of contact binaries. *Astron. J., 127,* 3023–3033.

Sheppard S. (2007) Light curves of dwarf plutonian planets and other large Kuiper belt objects: Their rotations, phase functions, and absolute magnitudes. *Astron. J., 134,* 787–798.

Spencer J., Stansberry J., Trafton L., Young E., Binzel R., and Croft S. (1997) Volatile transport, seasonal cycles, and atmospheric dynamics on Pluto. In *Pluto and Charon* (S. Stern and D. Tholen, eds.), p. 435. Univ. of Arizona, Tucson.

Stellingwerf R. (1978) Period determination using phase dispersion minimization. *Astron. J., 224,* 953–960.

Tegler S., Romanishin W., Consolmagno G., Rall J., Worhatch R., Nelson M., and Weidenschilling S. (2005) The period of rotation, shape, density, and homogeneous surface color of the Centaur 5145 Pholus. *Icarus, 175,* 390–396.

Trilling D. and Bernstein G. (2006) Light curves of 20–100 km Kuiper belt objects using the Hubble space telescope. *Astron. J., 131,* 1149–1162.

Wall J. and Jenkins C. (2003) *Practical Statistics for Astronomers.* Cambridge Univ., Cambridge.

Weidenschilling S. (1980) Hektor — Nature and origin of a binary asteroid. *Icarus, 44,* 807–809.

Weidenschilling S. (1981) How fast can an asteroid spin. *Icarus, 46,* 124–126.

Yeomans D., Barriot J., Dunham D., Farquhar R. W., Giorgini J. D., et al. (1997) Estimating the mass of asteroid 253 Mathilde from tracking data during the NEAR flyby. *Science, 278,* 2106–2109.